INT. J. NUM. METH. HEAT FLUID FLOW, VOL. 2, 139–154 (1992)

SIMULATION OF TRANSIENT THREE-DIMENSIONAL NATURAL CONVECTION AND SATURATED POOL BOILING

K. A. ELRAIS, W. ECKERLE*, G. AHMADI AND A. H. ERASLAN†

Department of Mechanical and Aeronautical Engineering, Clarkson University, Potsdam, NY 13699, USA

ABSTRACT

A three-dimensional, two-phase computational model for simulating boiling-enhanced mixed convection in free-surface flows is presented. The associated constitutive models for the thermophysical and transport properties are described. A computational model incorporating the discrete-element analysis was used to simulate the multi-dimensional, two-phase flow around a heated chip in a test tank filled with Freon-(R113). Two and three-dimensional simulations of both natural convection and nucleate boiling heat transfer regimes are presented. The velocity field, the temperature distribution, and the vapour concentration profiles are evaluated and discussed. The simulated heat fluxes are compared with the available experimental data. While the heat fluxes from the two-dimensional simulation agree with the fluxes calculated for the three-dimensional case, the flow in the tank is essentially three-dimensional. The results show that there are secondary flows which cannot be captured by a two-dimensional model. The heat flux in the boiling heat transfer regime is only about ten times larger than that in the natural convection regime due to the small vapour concentration in tank.

KEY WORDS Discrete element method ICEMER code Simulated heat fluxes Natural convection

INTRODUCTION

Analysis of boiling heat transfer is important because of its numerous industrial applications. Extensive reviews of the earlier and recent developments were provided by Tong[1], Bergles *et al.*[2,3], Kays and Perkins[4], Rohsenow and Hartnett[5], Grigull[6], Van Stralen and Cole[7] and Collier[8]. Recent developments in the area of computational fluid mechanics have provided several computational models for analyzing complex flows. Reviews of some of the available codes were given by Johnson[9], Chow[10] and Anderson *et al.*[11]. In here, only features of some of the earlier work directly relevant to the present study are described.

Developing a computational scheme for analysing time dependent viscous flows with a free surface was initiated by Harlow and Welch[12]. Further developments were carried out by Hirt and Shannon[13], Nichols and Hirt[14] and Spraggs and Street[15] who have considered three-dimensional flow regions. In their scheme, the successive overrelaxation method is used to solve the Poisson equation for the pressure at every time step. Tatom and Smith[16] developed a computational algorithm using the non-staggered finite difference method which calculates all flow variables at the same computational point of the unequally spaced grid system. They used orthogonal curvilinear coordinates and the Boussinesq approximation in their formulation. A

* Cumming Engine Company, Box 3005, Columbus, IN 47202, USA.
† AHE and Associates, Tullahoma, TN 37388, USA.

0961–5539/92/020139–16$2.00

Received June 1991

transient three-dimensional computational model, which utilizes the staggered-mesh space-differencing scheme similar to the MAC (marker and cell) method, was developed by Sicilian and Hirt[17]. A timewise explicit numerical integration scheme was used in the computational model, and the pressure distribution on the free surface and in the flow region was calculated by an iterative procedure at every time step.

The TEACH code has been used extensively in industrial applications. A review of the historical development as well as a new advanced version of the TEACH code was described by Lilley and Rhode[18]. The solution procedure involves an implicit line-by-line relaxation technique and requires the inversion of a tridiagonal matrix for updating the variables. The pressure is evaluated from the iterative solution of the corresponding Poisson equation. The computational schemes of the recent commercially available FLUENT and PHOENIC codes are similar to the TEACH code. Extensive applications of the PHOENIC code were described in Reference 19.

The spectral computational method has been used recently for direct simulation of turbulence by Moin and Kim[20], among others. Recently, Karniadakis[21] used the spectral method for simulating the transient forced convection heat transfer for a two-dimensional flow around a cylinder in an unbounded domain for Reynolds numbers up to 200. Although the spectral method appears to be a promising technique, its applications have been limited to low Reynolds number flows.

Eraslan *et al.*[22] developed a computer code (FLOWER) for simulating transient three-dimensional flow problems in complex geometries of coastal regions. The computational algorithm is based on the discrete-element method (DEM) developed by Eraslan[23], Eraslan and Tov[24] and Eraslan[25]. It also uses the timewise explicit, composite, multi-time step method. The computational algorithm of the FLOWER code utilizes the two horizontal components of the momentum equation for evaluating the horizontal components of velocity. The vertical component of velocity is obtained by algebraically integrating the discretized form of the conservation of mass equation along the vertical direction. The pressure is evaluated from the vertical component of the momentum equation. Therefore, the algorithm avoids the solution of the computationally intensive Poisson equation for pressure.

In this study, the formulation of a transient, two-phase, multi-dimensional computational code (ICEMER) is described. The computational model, which is based on the FLOWER code and utilizes the DEM, is capable of analysing two- and three-dimensional two-phase (liquid–vapour) free-surface flows in complex regions with heat and mass transfer. The developed model is used to simulate the flow field and the temperature and vapour concentration profiles in a test tank with a vertical heater under natural convection and nucleate boiling conditions. Comparisons are made with the available experimental data.

There were several reasons for studying the problem of convection in tank with a heated chip. First, it was a challenging and computationally demanding problem. The results were also of practical interest to the field of liquid cooled electronics. In addition, the experimental counter part study was available in the literature for comparison and test of accuracy.

COMPUTATIONAL MODEL

Governing equations

The formulation of the computational model includes a general two-phase liquid–vapour mixture model. The average (mass) density of the mixture ρ is given as the sum of the mean density of the liquid phase ρ_f and the mean density of the vapour phase ρ_g:

$$\rho = \rho_f + \rho_g \tag{1}$$

It should be emphasized that the mean density of a phase is defined as the mass of that phase per unit volume of the mixture. The concentrations (mass-fractions) of the two phases are defined as:

$$C_g = \frac{\rho_g}{\rho} \qquad C_f = \frac{\rho_f}{\rho} \tag{2}$$

where C_g and C_f are the concentrations of the vapour and fluid phases, respectively. According to the definition of the mixture density, then,

$$C_g + C_f = 1 \tag{3}$$

Note that, for the saturation temperature, C_g becomes identical to 'quality' which is commonly used in thermodynamics text books. However, the present formulation allows for the existence of liquid–gas mixtures away from saturation temperature, and hence, in principle, it is applicable to bubbly fluids and other two-phase flows.

In a two-phase mixture, the mean velocities of the liquid and vapour are generally different. The mass average velocity for the mixture is defined as:

$$\vec{V} = \frac{\rho_f \vec{V}_f + \rho_g \vec{V}_g}{\rho_f + \rho_g} \tag{4}$$

The mean velocities of the liquid and the vapour may be restated as:

$$\vec{V}_f = \vec{V} + \vec{v}_f^* \tag{5a}$$

$$\vec{V}_g = \vec{V} + \vec{v}_g^* \tag{5b}$$

where $\vec{v}_f^*$ and $\vec{v}_g^*$ are the diffusion velocities. Equations (4) and (5) imply that:

$$\rho_f \vec{v}_f^* + \rho_g \vec{v}_g^* = 0 \tag{6}$$

that is, for a binary mixture, the vapour diffusion flux and the liquid diffusion flux are equal in magnitude and are opposite in direction.

The statement of the mass conservation principle for the fluid phase in integral form is given as:

$$\frac{\partial}{\partial t}\iiint_v \rho_f \, dv + \iint_A (\tilde{\rho}_f \vec{V}_f)\cdot \hat{n} \, dA = \iiint_v \dot{\rho}_f \, dv \tag{7}$$

Similarly, the mass conservation principle for the vapour phase is given by:

$$\frac{\partial}{\partial t}\iiint_v \rho_g \, dv + \iint_A (\tilde{\rho}_g \vec{V}_g)\cdot \hat{n} \, dA = \iiint_v \dot{\rho}_g \, dv \tag{8}$$

where $\dot{\rho}_f$ and $\dot{\rho}_g$ denote the generation rates of the liquid and the vapour, respectively. Here ($\tilde{}$) indicates that an 'upwind-differencing' scheme in the discrete-element analysis must be used. Adding (7) and (8), the integral form of the equation of conservation of mass for the mixture follows:

$$\frac{\partial}{\partial t}\iiint_v \rho \, dv + \iint_A (\tilde{\rho}\vec{V})\cdot \hat{n} \, dA = 0 \tag{9}$$

where it is assumed that the net mass generation rate is zero:

$$\dot{\rho}_f + \dot{\rho}_g = 0 \tag{10}$$

The conservation principle for the vapour-mass fraction (concentration) may be obtained by substituting (2) and (5b) into (8). Thus,

$$\frac{\partial}{\partial t}\iiint_v (\rho C_g) dv + \iint_A (\tilde{\rho} C_g)\tilde{\vec{V}}\cdot \hat{n} \, dA = \iiint_v \rho \dot{C}_g \, dv + \iint_A g_{f/g}^{*\prime\prime}\cdot \hat{n} \, dA \tag{11}$$

Here, $\dot{C}_g$ is the rate of vapour-mass fraction generation and $g_{f/g}^{*\prime\prime}$ represents the vapour-mass (diffusion) flux defined as:

$$g_{f/g}^{*\prime\prime} = -(\tilde{\rho} C_g) v_g^* \tag{12}$$

The x-component of the momentum principle for the liquid-phase is:

$$\frac{\partial}{\partial t}\iiint_v \rho_f V_{f,x}\,dv+\iint_A (\tilde{\rho}_f \tilde{V}_{f,x})\vec{V}\cdot\hat{n}\,dA$$
$$=\iint_A p_f(-\hat{n})\cdot\hat{u}_x\,dA+\iint_A \overline{\sigma^{*''}_{f,nx}}\,dA+\iiint_v r_{cg,f,x}\,dv+\iiint_v r_{f/g,x}\,dv+\iiint_v \dot{\rho}_f v^*_{f,x}\,dv \quad (13)$$

and the x-component of the momentum principle for vapour-phase is:

$$\frac{\partial}{\partial t}\iiint_v \rho_g V_{g,x}\,dv+\iint_A (\tilde{\rho}_g \tilde{V}_{g,x})\vec{V}\cdot\hat{n}\,dA$$
$$=\iint_A p_g(-\hat{n})\cdot\hat{u}_x\,dA+\iint_A \overline{\sigma^{*''}_{g,nx}}\,dA+\iiint_v r_{cg,g,x}\,dv+\iiint_v r_{g/f,x}\,dv+\iiint_v \dot{\rho}_g v^*_{g,x}\,dv \quad (14)$$

Here, $\overline{\sigma^{*''}_{f,nx}}$ is the x-component of the viscous stress of the liquid-phase, $r_{cg,f,x}$ is the x-component of body force acting on the liquid-phase, and $r_{f/g,x}$ is the x-component of the interaction force of the vapour-phase acting on the liquid-phase. When subscript f is replaced by g, similar definitions hold for the vapour phase.

The total (mixture) pressure p is defined as the sum of the liquid and vapour pressures, i.e.,

$$p=p_f+p_g \quad (15)$$

The x-component of the viscous stress of the two-phase mixture $\overline{\sigma^{*''}_{f/g,x}}$ acting on a surface in the flow may be considered as the sum of the viscous stresses of the liquid and the vapour phases, i.e.,

$$\overline{\sigma^{*''}_{f/g,x}}=\overline{\sigma^{*''}_{f,nx}}+\overline{\sigma^{*''}_{g,nx}} \quad (16)$$

Similarly, the x-component of the mixture body force $r_{cg,x}$ is given as:

$$r_{cg,x}=r_{cg,f,x}+r_{cg,g,x} \quad (17)$$

Adding (13) and (14), and substituting (15)–(17) results in:

$$\frac{\partial}{\partial t}\iiint_v \rho V_x\,dv+\iint_A (\tilde{\rho}_f \tilde{V}_x)\vec{V}\cdot\hat{n}\,dA$$
$$=\iint_A p(-\hat{n})\cdot\hat{u}_x\,dA+\iint_A \overline{\sigma^{*''}_{nx}}\,dA+\iiint_v r_{cg,f,x}\,dv+\iiint_v \dot{\rho}_g v^*_{g,x}\left(1+\frac{\rho_g}{\rho_f}\right)dv \quad (18)$$

where

$$\overline{\sigma^{*''}_{nx}}=\overline{\sigma^{*''}_{f/g,x}}-\tilde{\rho}v^*_g v^*_{g,x}\left(1+\frac{\rho_g}{\rho_f}\right) \quad (19)$$

and

$$(\dot{\rho}_f v^*_{f,x}+\dot{\rho}_g v^*_{g,x})=\dot{\rho}_g v^*_{g,x}\left(1+\frac{\rho_g}{\rho_f}\right) \quad (20)$$

are used. The y and z components of the momentum equation may be obtained in a similar fashion.

The equation of conservation of energy for the mixture is given as:

$$\frac{\partial}{\partial t}\iiint_v \rho u_T\,dv+\iint_A (\tilde{\rho}\tilde{u}_T)\vec{V}\cdot\hat{n}\,dA=\iint_A q_T\cdot(-\hat{n})dA-\Delta u^*_{f/g}\iiint_v \dot{\rho}_g\,dv+\iiint_v p\vec{V}\cdot(-\hat{n})dA \quad (21)$$

where u_T is the mixture internal energy per unit mass, $\Delta u^*_{f/g}$ is the latent heat of vaporization, and q_T is the mixture heat diffusion vector which includes conduction in the liquid and the vapour phases as well as the energy fluxes due to mass diffusion.

Computational DEM equations

The DEM utilizes a novel composite-space-splitting (CSS) algorithm which considers four partly overlapping half-elements in the horizontal (x, y) plane for each element. Accordingly, two half-elements are used for evaluating the x and y components of velocity vector in each element in the layers as shown in *Figure 1*.

The discretized equations for the x-component of velocity $V_{x;i\mp\frac{1}{2},j,l}$ at the middle of the half-elements are obtained from the integral form of momentum principle as given by (18). Accordingly,

$$\frac{\partial}{\partial t}V_{x,i\mp\frac{1}{2},j,l}=\tilde{\bar{\Delta}}_{C,V,x;i\mp\frac{1}{2},j,l}+\bar{\Delta}_{P,V,x;i\mp\frac{1}{2},j,l}+$$

$$\bar{\Delta}_{D,V,x;i\mp\frac{1}{2},j,l}+\bar{\Delta}_{f/g,V,x;i\mp\frac{1}{2},j,l}+\bar{\Delta}_{CG,V,x;i\mp\frac{1}{2},j,l}+\tilde{\bar{\Delta}}_{I/D,V,x;i\mp\frac{1}{2},j,l} \tag{22}$$

Thus, for calculating $V_{x;i\mp\frac{1}{2},j,l}$, the six DEM operators corresponding to momentum convection, pressure force, momentum diffusion, vapour generation induced momentum, gravitational force and interaction force must be evaluated. The discretized equation for the y-component of velocity, $V_{y;i,j\mp\frac{1}{2},l}$ is obtained in a similar fashion. Details may be found in References 22 and 26.

The integral form of the conservation of mass principle, as given by (9), is used for obtaining the z-component of the velocity vector in the interior elements. The same equation is utilized in the surface layer for evaluating the elevation of the free surface. The discretized form of the mass conservation equation in the latter case is formally given as:

$$\frac{\partial}{\partial t}h_{i,j}=\tilde{\bar{\Delta}}_{C,h;i,j}+\tilde{\bar{\Delta}}_{I/D,h;i,j}+\bar{\Delta}_{\rho,h;i,j} \tag{23}$$

where $h_{i,j}$ is the free surface elevation at the centre of the i,jth surface element. The various DEM operators are defined as noted before.

The z-component of the integral form of the momentum principle is used to obtain the set of DEM equations for the pressure on the z-downstream enclosure surface $(i,j,l-\frac{1}{2})$ of the element (i,j,l):

$$p_{i,j,l-\frac{1}{2}}=p_{i,j,l+\frac{1}{2}}+\bar{\Delta}_{t,V,z;i,j,l}+\tilde{\bar{\Delta}}_{C,V,z;i,j,l}+\bar{\Delta}_{D,V,z;i,j,l}+\bar{\Delta}_{f/g,V,z;i,j,l}+\bar{\Delta}_{CG,V,z;i,j,l}+\tilde{\bar{\Delta}}_{I/D,V,z;i,j,l} \tag{24}$$

The terms on the righthand side of (24) are the discrete-element operators for time variation, momentum convection, momentum diffusion, vapour generation, gravitational force, and interaction force for the z-component velocity vector.

The integral form of thermal-energy conservation principle as given by (21) is used to obtain the set of DEM equations for evaluating the temperature $T_{i,j,l}$ in element (i,j,l):

$$\frac{\partial}{\partial t}T_{i,j,l}=\tilde{\bar{\Delta}}_{C,T;i,j,l}+\bar{\Delta}_{D,q,T;i,j,l}+\bar{\Delta}_{f/g,T;i,j,l}+\bar{\Delta}_{I/D,T;i,j,l} \tag{25}$$

The four DEM operators on the righthand side of (25) correspond to convection, diffusion, phase transformation and interaction energy supply. Similarly, (11) is used for obtaining the DEM equation for the vapour mass fraction $C_{g;i,j,l}$ in the element (i,j,l), that is,

$$\frac{\partial}{\partial t}C_{g;i,j,l}=\bar{\Delta}_{D,g;i,j,l}+\bar{\Delta}_{t,g;i,j,l}+\bar{\Delta}_{I/D,g;i,j,l} \tag{26}$$

The explicit expressions for the various DEM operators corresponding to convection, diffusion, phase transformation, interaction etc. may be found in Reference 26.

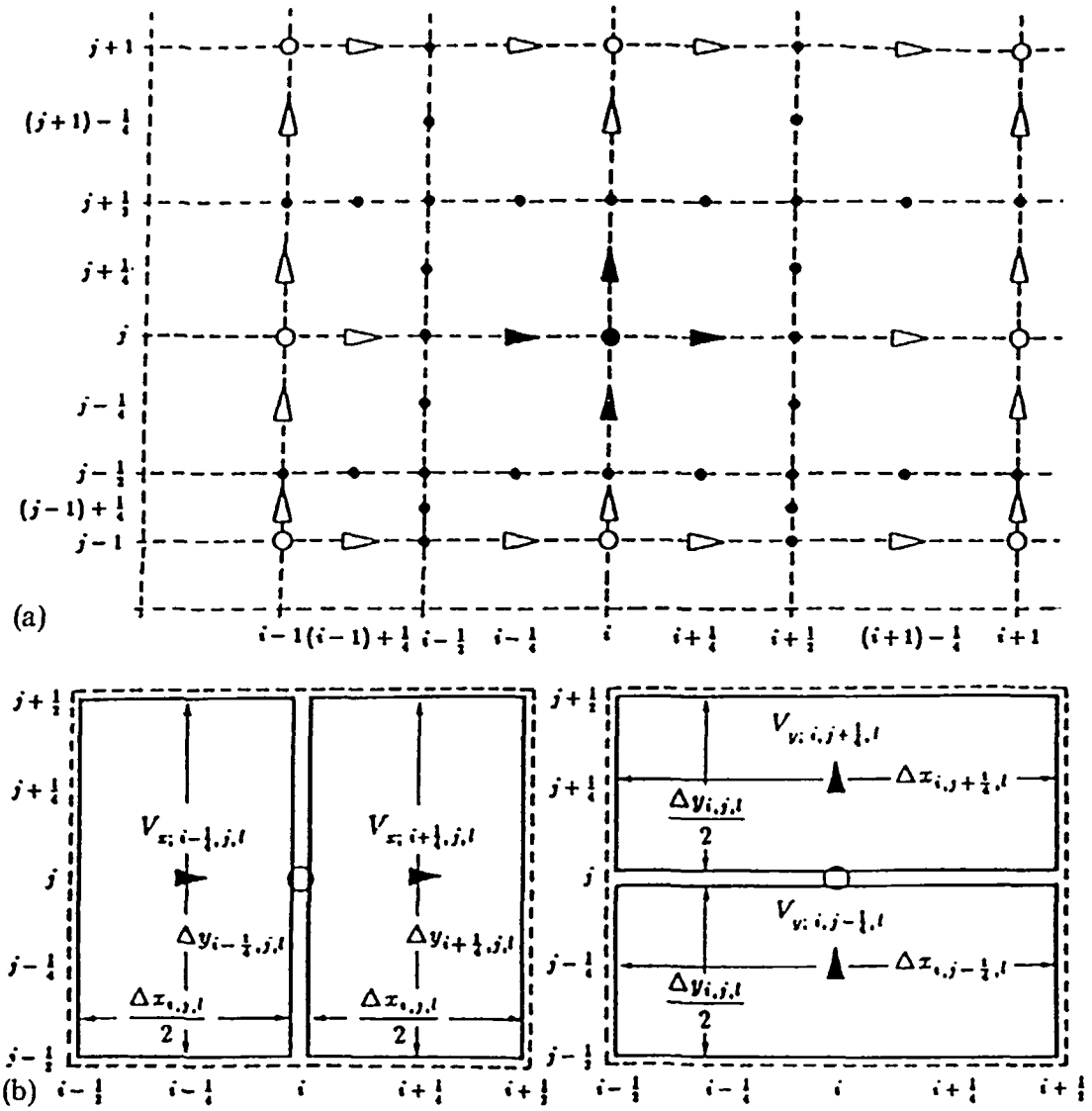

Figure 1 Simple-element composite-space-splitting (CSS) algorithm of DEA. (a) Computation and interpolation in (x, y) plane; (b) half elements for calculations of x- and y-components of velocity. ○, Computation locations for $h_{i,j}$, $T_{i,j,l}$, $P_{i,l-\frac{1}{2}}$, $V_{x,i,j,l+\frac{1}{2}}$; ▶, computation locations for $V_{x,i\mp 1/4,j,l}$; ▲, computation locations for $V_{x,i\mp\frac{1}{2},j,l}$; ●, interpolation (linear and upwind) locations

Phase-transformation model

The rate of vapour generation is calculted by a linear phase-transformation model which explicitly allows for non-equilibrium evaporation or condensation:

$$\dot{C}_g = R_{f/g} C_f - R_{g/f} C_g = R_{f/g}(1 - C_g) - R_{g/f} C_g \tag{27}$$

where $R_{f/g}$ and $R_{g/f}$ represent phase-transformation rates for liquid to gas and for gas to liquid, respectively. Note that vapour is generated only in the temperature range between T_f and T_g. Beyond this temperature range, the rate of vapour generation is zero, i.e.,

$$\text{for } T \leqslant T_f\text{: } C_g=0 \quad \text{and} \quad \dot{C}_g=0 \tag{28a}$$

$$\text{for } T \geqslant T_g\text{: } C_g=1 \quad \text{and} \quad \dot{C}_g=0 \tag{28b}$$

In the temperature range ($T_f < T < T_g$), liquid–vapour phase transformation rates are formulated according to modified Arrhenius expressions:

$$R_{f/g}=D_{f/g}[(T-T_f)/(T_g-T_f)]^{d_{f/g}}\cdot\exp\{E_{f/g}[(T-T_f)/(T_g-T_f)]^{e_{f/g}}\} \tag{29a}$$

$$R_{g/f}=D_{g/f}[(T_g-T)/(T_g-T_f)]^{d_{g/f}}\cdot\exp\{E_{g/f}[(T_g-T)/(T_g-T_f)]^{e_{g/f}}\} \tag{29b}$$

where coefficients, $D_{f/g}$, $E_{f/g}$, and $D_{g/f}$, $E_{g/f}$, and powers of temperature-dependent terms, $d_{f/g}$, $e_{f/g}$, and $d_{g/f}$, $e_{g/f}$, are constants associated with phase transformation characteristics of the fluid. The values of parameters for Freon-(R113) were described[26], where it was shown that the phase transformation model given by (29) is consistent with the experimentally observed hysteresis variation during phase change.

Special features of the ICEMER code

A detailed description of the ICEMER code was provided by Elrais[26]. Therefore, only few important features of the ICEMER code are listed in here. The ICEMER code is an advanced version of the FLOWER code developed earlier by Eraslan *et al.*[22]. The computational code is based on the discrete-element method (DEM) and includes the following special features:

(1) the computational algorithm has the capability of simulating transient two-phase (liquid–vapour), multidimensional free-surface flow problems in regions with complex boundaries;

(2) the computational algorithm considers the effects of variations of thermophysical and transport properties with temperature, pressure and vapour concentration;

(3) the mathematical formulation does not include the restrictive hydrostatic pressure assumption or the rigid-lid approximation used in many of the existing codes[16,27–29]. The discrete element formulation considers all the terms associated with the vertical momentum transport equation;

(4) the special mathematical formulation of the ICEMER code, like the FLOWER code, allows for its application in reduced two- or one-dimensional forms without requiring any modification in the general structure of the computer code;

(5) special computational features include the geometrically accurate composite space splitting (CSS) discretization algorithm of the DEM, and the composite time splitting (CTS) explicit integration algorithm. The numerical integration of the convective transport terms is formulated as a single time step, two level algorithm, with second order directional transportive upwind interpolation (DTUI), which minimizes the numerical dispersion effects (including artificial viscosity) and guarantees stability. The numerical integration of the non-convective transport terms is formulated as a two time step, three time level algorithm which guarantees the stability of the solutions. The maximum allowable time step of numerical integration satisfies the CFL criterion. The computational model, generally, requires less CPU time than other three-dimensional models[13–15,27–29]. Also, its timewise explicit numerical integration algorithm can include the effects of surface gravity waves.

SIMULATIONS OF NATURAL CONVECTION AND BOILING HEAT TRANSFER FLOW REGIMES

Park and Bergles[30] experimentally studied natural convection and boiling heat transfer conditions in a test tank with a heated microchip as shown in *Figure 2*. Their experiments were performed in an insulated covered tank with a cross-section of 273 mm × 127 mm and a 152 mm height. A 60 mm × 5.6 mm heater was mounted on a substrate 60 mm below the free surface and 60 mm

from the side of the tank. The working fluid was Freon-(R113) (trichlorotrifluoroethane). Freon-(R113) was selected because its properties are similar to those of dielectric liquids commonly used for immersion cooling of microelectronic components.

The ICEMER code was used to calculate the flow and thermal conditions in the test tank of Park and Bergles. The boundary conditions were selected to simulate the conditions of the experimental studies as closely as possible. The heater temperature was assumed to be uniform due to the small size of the heater. The space above the Freon-(R113) surface was taken to be at atmospheric pressure. The walls of the tank were considered to be insulated and impermeable.

The boundary condition used in the simulation for the upper surface in the simulation is quite different from the experimental condition of Park and Bergels. In the experiment, the tank was closed and vapour could communicate with the surrounding only through a reflux condenser. As noted before, the ICEMER computational code is for free surface flows. Thus, free surface condition had to be prescribed at the upper surface. Here, a simple convective boundary condition for the heat flux at the free surface was assumed, i.e.,

$$q_h = h_c(T_{env} - T_{liq}) \tag{30}$$

where T_{env} is the room temperature (25°C), T_{liq} is the temperature of the liquid at the free surface, and h_c is the free surface convective heat transfer coefficient ($10.04\,J/m^2.K^{31}$. Similarly, the boundary condition for the vapour mass flux at the free surface of the tank in the boiling heat transfer regime was defined by:

$$q_c = K_c(C_{env} - C_g) \tag{31}$$

where K_c is the mass transfer coefficient of vapour into air ($0.12 \times 10^{-2}\,m/s^{31}$, C_{env} is the ambient vapour concentration (assumed negligible), and C_g is the vapour concentration at the free surface of the tank. The initial vapour concentration inside the tank at the start of the numerical simulations was set to zero.

The flow field, the temperature profiles and the vapour concentration contours were evaluated for both natural convection and boiling heat transfer regimes. The results for the steady state regime are presented in graphical form and discussed in the following sections.

Two-dimensional simulations

The two-dimensional simulations were carried out in a tank model with a 60 mm axial length and a 152 mm height. The heater was located 60 mm below the free surface. A staggered grid with eight elements in the horizontal and vertical directions as shown in *Figure 3* was used. The location of heater is also shown in this Figure. The initial liquid temperature was 25°C in the natural convection simulations. The boiling heat transfer simulations were completed under saturated boiling conditions with an initial temperature of 46.8°C, which was 0.3°C above the saturation temperature. All results are shown for a heater temperature of 70°C.

The velocity vector plots in the natural convection and boiling heat transfer regimes are shown in *Figure 4*. The abscissa in this Figure is the distance from the heater. The plot shows an upward flow near the heater due to the generation of convective currents by the high temperatures in the vicinity of the heater. The velocity decreases gradually as the flow approaches the free surface of the tank. The flow then moves in a clockwise direction leading to a rather large region of circulating flow in the tank. For the boiling condition, the upward flow near the heater is stronger than the upward flow in the natural convection heat transfer case. This stronger flow can be attributed to the buoyancy induced by the formation of vapour during boiling. In this case, the circulation zone formed by the convective currents and the vapour buoyancy effects spreads over the entire tank and forms a large steady vortex.

Constant temperature contours in the natural convection and boiling heat transfer regimes are shown in *Figure 5*. For the natural convection case, the isotherms indicate 0.02, 0.05, 0.1, 0.15 and 0.18°C temperatures above the saturation temperature of the Freon-(R113) which is 46.5°C. The isotherm pattern reflects the expected heat convection effects. The Freon-(R113)

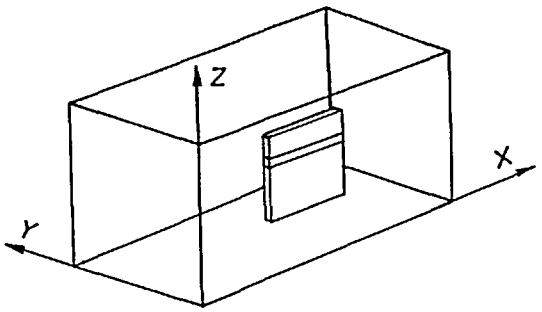

Figure 2 Schematic of the experimental tank

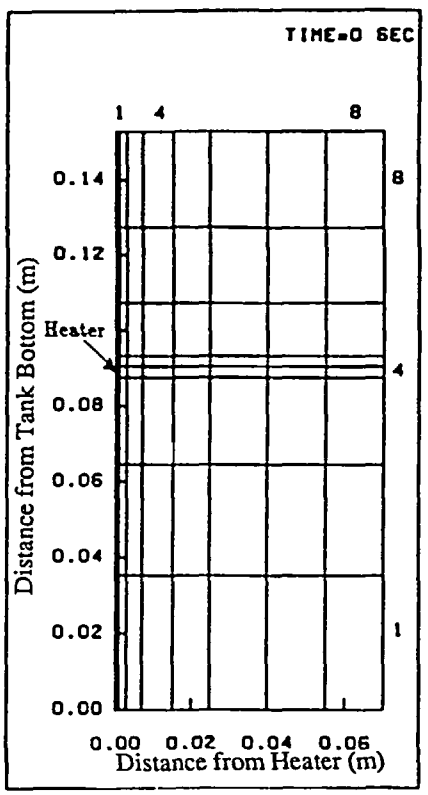

Figure 3 DEA grid for two-dimensional simulation

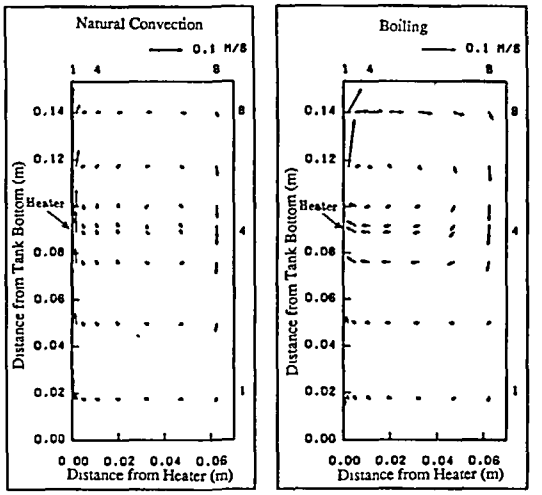

Figure 4 Velocity vector plots for two-dimensions

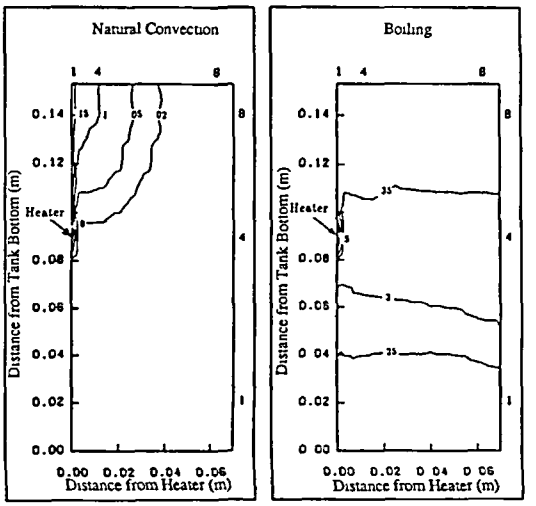

Figure 5 Isotherms for two-dimensional simulation

temperature rises in a thin layer with a very steep gradient near the heater surface. The temperature is highest in the quadrant near the chip above the heater where flow moves upward toward the free surface. As the flow moves away from the chips near the free surface, the temperature decreases as shown in the Figure.

The isotherms for the boiling heat transfer regime shown in *Figure 5b* indicate 0.25, 0.3, 0.35, 0.4 and 0.5°C above the saturation temperature of the Freon-(R113). The temperature contours show a general increase of fluid temperature when compared to the natural convection regime for the same heater temperature. A somewhat higher temperature also appears near the free surface of the test tank due to a continuous upward migration of vapour. The vortex circulation leads to higher temperatures throughout the tank.

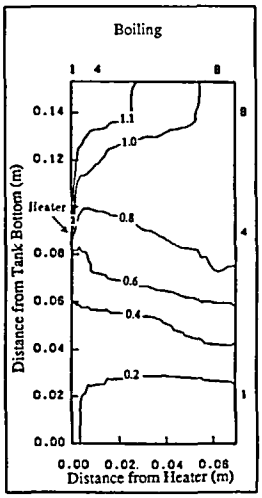

Figure 6 Vapour concentration for two-dimensional simulation (values of vapour contours in %)

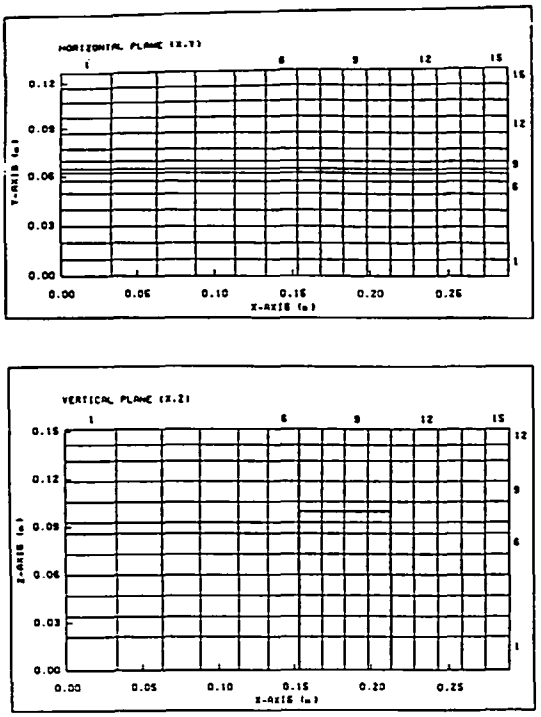

Figure 7 DEA grid for three-dimensional simulation

Vapour concentration profiles in the tank in the boiling heat transfer regime are shown in *Figure 6*. The vapour formed around the heater tends to migrate upward leading to a higher vapour concentration near the free surface. The vapour concentration gradually decreases from the free surface toward the bottom of the tank. Comparison of the heat fluxes with experimental and empirical data for both natural convection and boiling heat transfer regimes are described in the subsequent section.

Three-dimensional simulations

A three-dimensional simulation of flow and thermal conditions in the tank was also conducted. A three-dimensional grid with fifteen elements in the x-direction, fifteen elements in the y-direction and twelve elements in the z-direction as shown in *Figure 7* was used in the simulation. Detailed results for the boiling heat transfer condition are only presented in this section. Similar results including those for the natural convection heat transfer regime were described in Reference 26.

Computer simulation results for the flow field in the (y,z) plane passing through the centre of the chip are shown in *Figure 8a*. The velocity vectors indicate relatively strong counter-rotating vortices on the sides of the chip. The circulation zones are spread over the entire width of the tank similar to the flow field shown in *Figure 4* for the two-dimensional simulation. The circulation of the three-dimensional simulation, however, is stronger. Relatively high vertical velocities next to the chip and the side of the tank are noticed.

The velocity vectors in the (x,z) plane (*Figure 8b*) also indicate strong upward flow near the chip. The flow to the right of the chip is vortical but a well formed vortex is not displayed by the vectors. Rather, with the exception of the free surface, a general movement of fluid toward the chip is indicated in this region. To the left of the chip, a small vortex can be seen near the free surface with a slow recirculating flow around it.

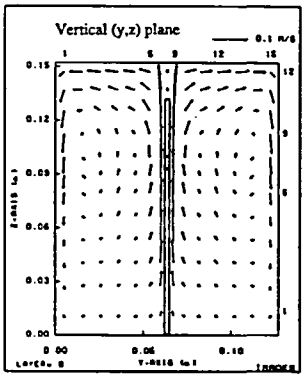

(a)

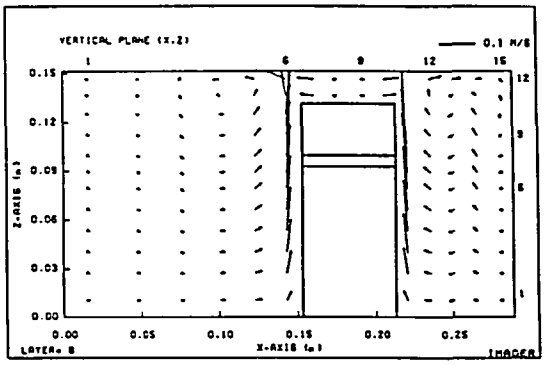

(b)

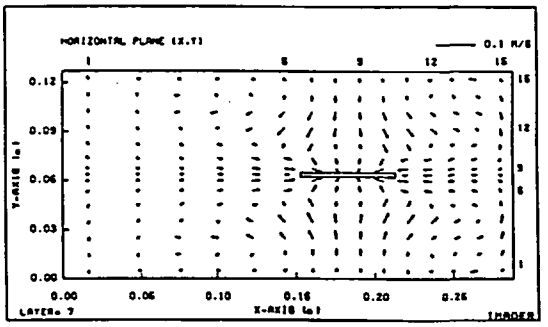

(c)

Figure 8 Velocity vector plots for three-dimensional simulation

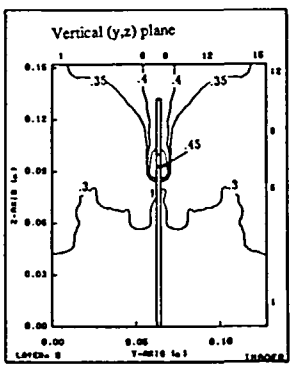

(a)

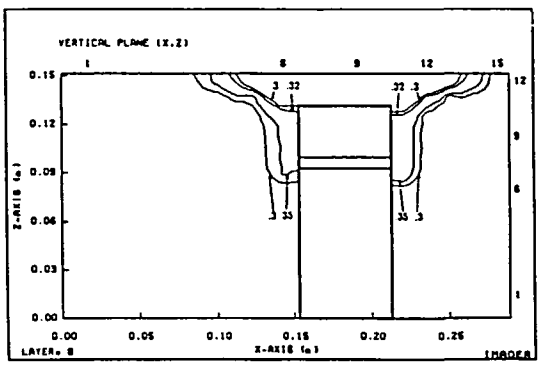

(b)

Figure 9 Isotherms for three-dimensional simulation

The general behaviour of the two phase flow pattern in the (x, y) plane containing the heater is displayed in *Figure 8c*. Flow toward the heater is apparent in this figure. Park and Bergles[30] have suggested that the regions of inward flow in the tank, such as those shown in *Figure 8c*, are generated by a circumferential flow pattern in which the lower density vapour-rich fluid migrates up to the free surface, leaving the incoming liquid-rich fluid to flow towards the heater. furthermore, the fluid velocity induced by the stream of vapour near the heat leads to an inherent 'forced' convective component in the boiling process. *Figure 8* also displays the three dimensionality of the flow in the tank, which the two-dimensional analysis cannot fully describe.

The temperature distributions in the boiling heat transfer regime in the (y, z) and (x, z) planes are shown in *Figure 9*. The temperature contour pattern in both planes is approximately the same. The continuous migration of vapour towards the free surface along with the vortex system interactions inside the tank have substantial effects on the temperature distribution. The localized

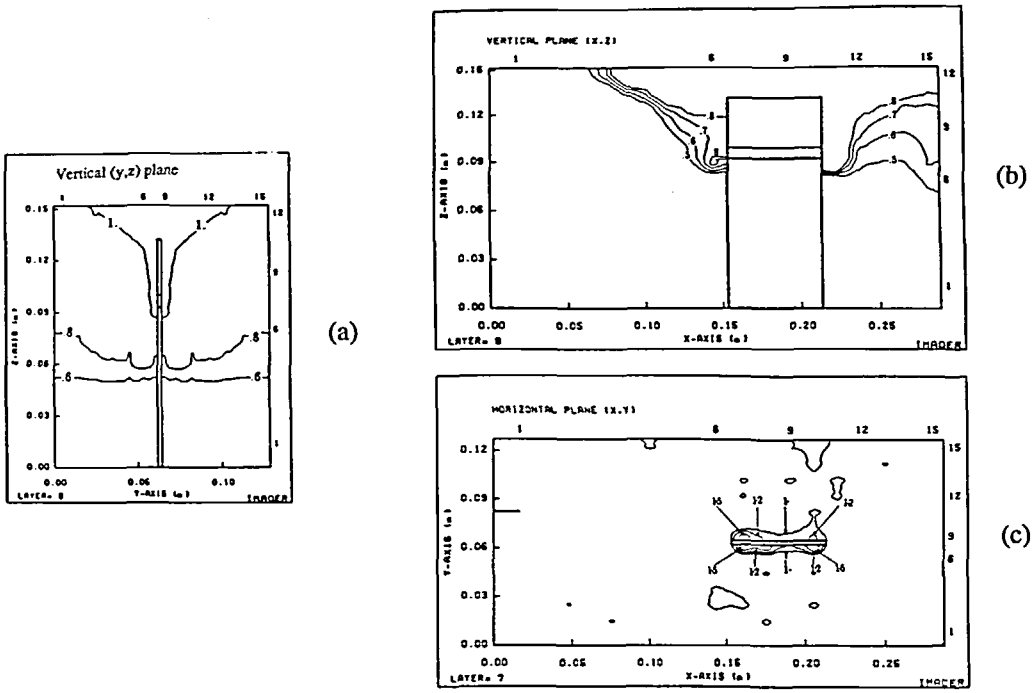

Figure 10 Vapour contours (%) for the three-dimensional simulation

effects of the three-dimensional vortices together with the horizontal and vertical temperature gradient interactions also lead to wavy isotherms and somewhat higher temperatures near the tank bottom and free surface in comparison with the two-dimensional temperature contours shown in *Figure 5*.

Vapour concentrations in the (y,z), (x,z) and (x,y) planes are shown in *Figure 10*. Buoyancy driven vapour flow patterns from the heater towards the free surface of the tank are indicated in both the (x,z) and (y,z) planes. As noted before, the vapour is mainly formed around the heater and tends to migrate toward the free surface of the tank forming a region of relatively high vapour density. Circulation sweeps in vapour near the free surface back towards the bottom of the tank. Therefore, high vapour concentration occurs in the region near the free surface and decreases gradually towards the bottom of the tank.

Figure 10a shows that although the vapour concentration near the heater is almost equal to the two-dimensional level shown in *Figure 6*, the vapour concentration distributions in the tank are different. This difference is attributed to the three-dimensional thermally induced convection caused by the presence of horizontal and vertical temperature gradients. Results for the vapour concentration in the (x,y) plane containing the heater are shown in *Figure 10c*. The value of the unlabelled contours in these Figures are for a concentration of 0.01. High concentration of vapour occurs near the heater and decreases rapidly with the distance from the heater. The three dimensionality of the flow is apparent in the asymmetry of the contours.

Boiling heat fluxes

The variation of the average heat flux for the four elements of the heater in the boiling heat transfer regime with time is shown in *Figure 11a*. The heat flux, which is nearly the same for the four elements, increases rapidly to about 1.03×10^5 w/m^2 in about 0.5 sec. The heat flux

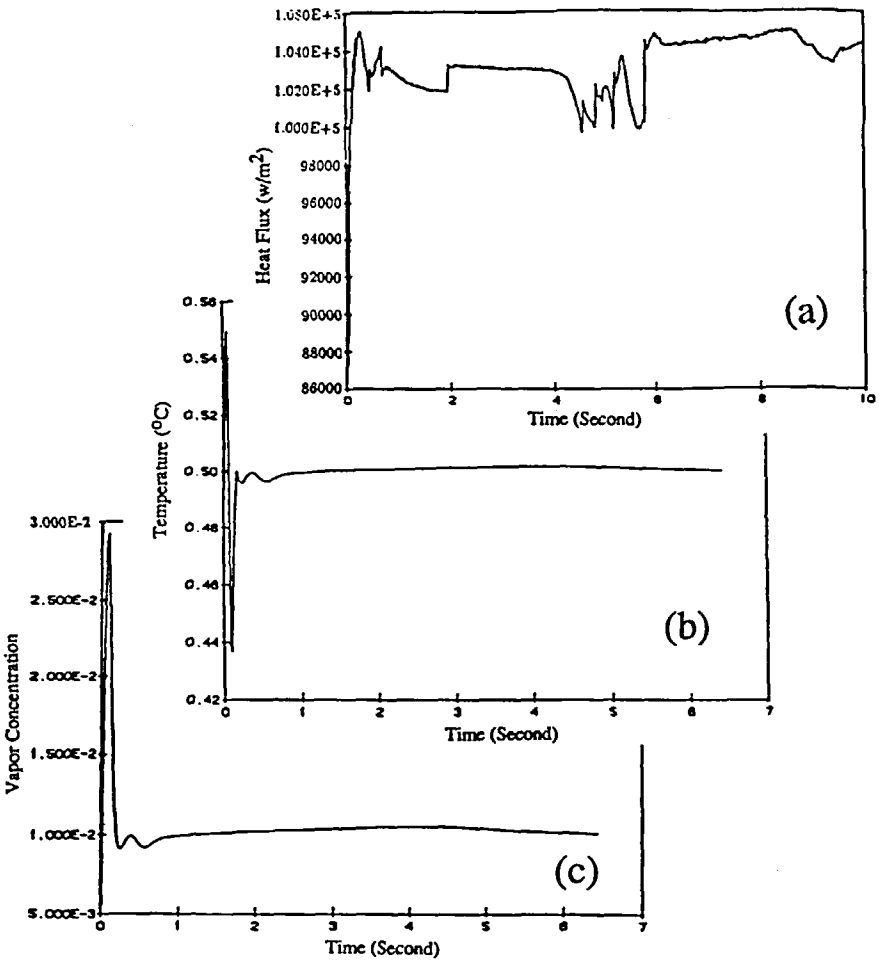

Figure 11 Time evolutions of heater heat flux, temperature and vapour concentration in the vicinity of the heated chip

exhibits a rather complex pattern of fluctuations with an amplitude of about 2500 w/m^2. The variation is possibly due to changing vortex circulation patterns following a thermal instability (non-uniform temperature distribution) in the flow region.

The variation of the temperature of the mixture in the element next to the heater is displayed in *Figure 11b*. The variation of the vapour concentration with time in this element is shown in *Figure 11c*. Initially, there is an increase in the vapour concentration and temperature next to the heater until the buoyancy force presumably becomes substantial and a relative rapid upward flow is generated. Subsequently, the vapour concentration next to the heater drops sharply and almost reaches a steady state limit. The fluid temperature also undergoes sharp variations before approaching to a steady state value of 0.5°C above the saturation temperature.

Comparison with data

The heat fluxes from numerical calculations for both the natural convection and boiling heat transfer regimes were evaluated from:

$$q=\kappa\frac{\partial T}{\partial x_i}+\dot{m}_g h_{fg} \qquad (i=1,2,3) \tag{43}$$

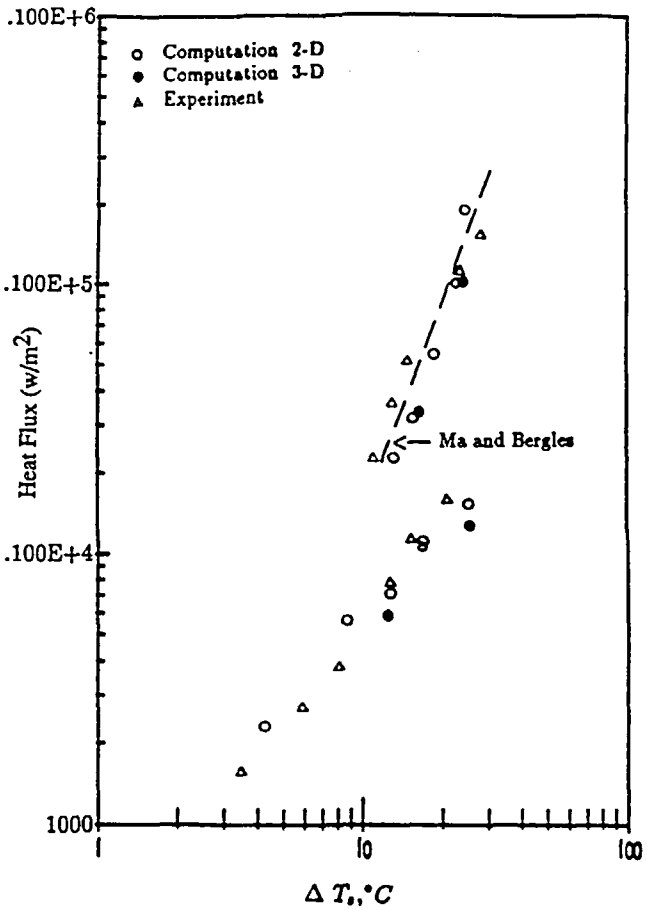

Figure 12 Comparison of the two- and three-dimensional results in the natural and boiling heat transfer regimes with experimental data

When $\dot{m}_g$ equals zero, (43) provides the heat flux due to natural convection. Numerical results for two-dimensional and three-dimensional simulations for different heater temperatures together with the experimental results of Ma and Bergles[32] (the broken line) and Park and Bergels[30] are shown in *Figure 12*. During their experiments, the steady-state temperature on the heater was measured for many different levels of heat flux. The heat flux data in *Figure 12* are plotted vs. the temperature difference between the heater temperature and the liquid saturation temperature. The results in *Figure 12* show that the numerical predictions of the two-dimensional and the three-dimensional simulations are in good agreement with experimental results. This agreement between the two- and three-dimensional simulations is consistent with the similar flow pattern calculated near the heater for these two cases. All the data show a rapid increase in heat flux with increasing heater temperature, typical of free convection and nucleate boiling. Heat fluxes in the boiling heat transfer regime are approximately an order of magnitude larger than the heat fluxes associated with the natural convection regime. This increase is also consistent with nucleate boiling where the effect of bubble formation leading to formation of jets and columns is not present.

CONCLUSIONS

Based on the presented results the following conclusions may be drawn:

(1) the simulated heat fluxes are in good agreement with the experimental data[30,32] for both the natural convection and the boiling heat transfer regimes;

(2) the heat fluxes in the boiling heat transfer regime are increased nearly tenfold over the heat fluxes in the natural convection regime;

(3) the heat fluxes calculated for the two- and three-dimensional cases are in agreement in both the natural convection and boiling heat transfer regimes. The conditions inside the tank are different due to the three-dimensional thermally induced convection caused by the presence of horizontal and vertical temperature gradients;

(4) relatively high vapour concentrations and temperatures were calculated near the heater and the free surface. These properties decrease gradually toward the bottom of the tank;

(5) the computational model ICEMER code has the capability to simulate transient, three-dimensional and two-phase problems in complex geometries.

NOMENCLATURE

A	area of a control volume
C	concentration
CSS	composite-space-splitting
CTS	composite-time-splitting
$D_{f/g}$	binary diffusion coefficient
$D_{f/g}, D_{g/f}$	coefficients in the phase-transformation submodel
$DTUI$	directional transportive upwind interpolation
$d_{f/g}, d_{g/f}$	coefficients in the phase-transformation submodel
$E_{f/g}, E_{g/f}$	coefficients in the phase-transformation submodel
$e_{f/g}, e_{g/f}$	coefficients in the phase-transformation submodel
$g^*_{f/g}$	mass diffusion flux
h	surface elevation
h_L	heat transfer coefficient
K_c	mass transfer coefficient
$\dot{m}_g$	rate of vapour mass generation
$\hat{n}$	unit vector
p	pressure
p_f, p_g	pseudo partial pressure
q_T	effective heat flux
$R_{f/g}$	phase transformation rate from liquid to gas
$R_{g/f}$	phase transformation rate from gas to liquid
r_{cg}	body force per unit volume
T	temperature
t	time
u	thermal specific energy
$\hat{u}_x$	unit vector in x direction
$\vec{V}$	mass-weighted average velocity
$\vec{V}_f, \vec{V}_g$	mass-weighted average phasic velocities
v	control volume
$\vec{v}^*$	diffusion velocity
x, y, z	space coordinates

Greek symbols

ρ	bulk density
ρ_f, ρ_g	mean phasic densities
$\Delta x, \Delta y, \Delta z$	element size in x, y and z direction
Δt	time step
$\bar{\Delta}_t$	time-variational DEM operator
$\bar{\Delta}_C$	convection DEM operator
$\bar{\Delta}_D$	diffusion DEM operator
$\bar{\Delta}_{f/g}$	phase change DEM operator
$\bar{\Delta}_{CG}$	body force DEM operator
$\bar{\Delta}_{I/D}$	interaction DEM operator
$\bar{\Delta}_P$	pressure DEM operator
$\bar{\Delta}_\rho$	densimetric DEM operator
$\Delta u^*_{f/g}$	latent heat of formation
$\overline{\sigma^{*\prime\prime}}$	viscous stress
ν	kinematic viscosity
μ	dynamic viscosity

Subscripts

b	boiling
f	liquid phase
g	vapour phase
i, j, l	element number in x, y and z direction
ref	reference value
srf	surface layer

Superscripts

$\tilde{(\ )}$	generalized 'upwind-differencing'
$\bar{(\ )}$	averaged term
n	time step number

ACKNOWLEDGEMENTS

The work of GA was partly supported by the DOE under Grant DE-GF22-91PC91297 and the New York State Science and Technology Foundation through the Center for Advanced Material Processing (CAMP) of Clarkson University. The use of Cornell University supercomputer facility is also gratefully acknowledged.

REFERENCES

1 Tong, L. S. *Boiling Heat Transfer and Two-Phase Flow*, Wiley, New York (1965)
2 Bergles, A. E., Chu, R. C. and Seely, J. H. Survey of heat transfer techniques applied to electronic equipment, *ASME paper, No. 72-WA/HT-39* (1972)
3 Bergles, A. E., Chu, R. C. and Seely, J. H. Survey of heat transfer techniques applied to electronic packaging, *Proc. Nat. Electron. Packag. Prod. Conf.*, pp. 370–385 (1977)
4 Kays, W. M. and Perkins, J. P. *Handbook of Heat Transfer*, McGraw-Hill, New York (1973)
5 Rohsenow, W. M. and Hartnett, J. P. *Handbook of Heat Transfer*, McGraw-Hill, New York (1973)
6 Grigull, H. *Heat Transfer in Boiling*, Academic Press, San Diego (1977)
7 Van Stralen, S. I. and Cole, R. *Boiling Phenomena*, Vols. 1, 2, McGraw-Hill, New York (1979)
8 Collier, J. G. *Convective Boiling and Condensation*, McGraw-Hill, New York (1981)
9 Johnson, B. H. *A Review of Numerical Reservoir Hydrodynamic Modeling*, Hydraulics Lab., US Army Engineer Waterways Exp. Station, Vicksburg, Miss (1981)
10 Chow, C. Y. *An Introduction to Computational Fluic Mechanics*, John Wiley, New York (1979)
11 Anderson, D. A., *et al. Computational Fluid Mechanics and Heat Transfer*, Hemisphere, Washington DC (1984)
12 Harlow, F. H. and Welch, J. W. Numerical calculation of time-dependent viscous incompressible flow of fluid with free surface, *Phys. Fluids* **8**, 2181–2189 (1965)
13 Hirt, C. W. and Shannon, J. P. Free surface stress conditions for incompressible flow, *J. Comput. Phys.* **2**, 403–411 (1968)
14 Nichols, B. D. and Hirt, C. W. Calculating three-dimensional free-surface flows in the vicinity of submerged and exposed structures, *J. Comput. Phys.* **12**, 234–246 (1973)
15 Spraggs, L. D. and Street, R. L. Three-dimensional simulation of thermally influenced hydrodynamic flows, *Report No. TR-190*, Dept. of Civil Eng., Stanford Univ. (1976)
16 Tatom, F. B. and Smith, S. R. *Three-Dimensional computer Simulation of Cold Water Inflow*, US Army Engineer Waterways Exp. Station, Vicksburg, Miss (1979)
17 Sicilian, J. M. and Hirt, C. W. *HYDR-3D a Solution Algorithm For Transient 3D Flows*, Flow Science (1985)
18 Lilley, D. G. and Rhode, D. L. A computer code for swirling turbulent axisymmetric recirculating flows in practical isotherms combustor geometries, *NASA Contractor Report 3442* (1982)
19 Markatos, N. C., Tatchell, D. G., Cross, M. and Rhodes, N. Numerical simulation of fluid flow and heat/mass transfer processes, *Lecture Notes in Engineering* **18**, Springer-Verlag, Berlin (1985)
20 Moin, P. and Kim, J. Numerical investigation of turbulent channel flow, *J. Fluid Mech.* **118**, 341–377 (1982)
21 Karniadakis, G. E. Numerical simulation of forced convection heat transfer from a cylinder in a crossflow, *Int. J. Heat Mass Transfer*, **31**, 107–118 (1988)
22 Eraslan, A. H., Lin, W. and Sharo, R. D. FLOWER: a computer code for simulating three-dimensional flow, temperature and salinity conditions in rivers, estuaries and coastal regions, *NUREG/CR-3172, ORNL/TM-840*. Oak Ridge National Laboratory, Oak Ridge, TN (1983)
23 Eraslan, A. H. Transient, two-dimensional, far-field model for thermal impact analysis of power plant discharges in coastal and offshore regions. Part 1, *ORNL-4940*, Oak Ridge Natl. Lab., Oak Ridge, TN (1974)
24 Eraslan, A. H. and Tov, M. S. A tidal transient, far-field model for offshore thermal discharges, *Trans. Am. Nucl. Soc.* **18**, 55 (1974)
25 Eraslan, A. H. Discrete-element models for thermal impact assessment of large power plants in estuaries and coastal regions, in *Proc. 12th Southeast. Semin. Therm. Sci., Charlottesville* (1976)
26 Elrais, K. A. Computer modeling of transient three-dimensional boiling enhanced mixed convection, *PhD Thesis* (Also *MIE Report No. 170*), Department of Mechanical and Industrial Engineering, Clarkson Univ., Potsdam (1988)
27 Lick, W. Numerical models of lake currents, *U.S. Report No. EPA-600/3-76-020*, EPA, Office of Research and Development, Environmental Research Lab., Duluth, MN (1976)
28 Blumberg, A. F. and Mellor, G. L. *A Coastal Ocean Numerical Model*, Geophysical Fluid Dynamics Program, Princeton Univ. (1978)
29 McMaster, W. H. and Gong, E. Y. PELEC-IC user's manual, Lawrence Livermore Laboratory, *Report No. UCRL-52609* (1980)
30 Park, K. A. and Bergles, A. E. Effects of the size of simulated microelectronic chips on boiling and critical heat flux, *ASME, HTD-57*, pp. 95–102 (1986)
31 Bolz, R. E. and Tuue, G. L. *Handbook of Tables for Applied Engineering Science*, CRC, Cleveland, OH (1985)
32 Ma, C. F. and Bergles, A. E. Boiling jet impingement cooling of simulated microelectronic chips, *ASME HTD-28*, pp. 3–10 (1983)